High-throughput screening identification of a small-molecule compound that induces ferroptosis and attenuates the invasion and migration of hepatocellular carcinoma cells by targeting the STAT3/GPX4 axis

QI HUANG[1,2*], JING LI[1-3*], MENGQING MA[1,2*], MINLING LV[1,2], RUI HU[1,2], JIALING SUN[1,2], XIN ZHONG[1,2], XINFENG SUN[1,2], WENXING FENG[1,2], WENFENG MA[1,2], WEI ZHANG[1,2], BOLIN ZHAN[1,2], ZHIYI HAN[1,2] and XIAOZHOU ZHOU[1-3]

[1]Department of Liver Disease, The Fourth Clinical Medical College of Guangzhou University of Chinese Medicine; [2]Department of Liver Disease, Shenzhen Traditional Chinese Medicine Hospital, Shenzhen, Guangdong 518033; [3]Macau University of Science and Technology, Faculty of Chinese Medicine, Taipa, Macao 999078, P.R. China

Received June 23, 2022; Accepted February 9, 2023

DOI: 10.3892/ijo.2023.5490

Abstract. Hepatocellular carcinoma (HCC) is a lethal malignancy. Although considerable efforts have been made in recent years regarding treatments, effective therapeutic drugs for HCC remain insufficient. In the present study, polyphyllin VI was identified as a potential therapeutic drug for HCC by screening natural herbal compounds. The therapeutic effects of polyphyllin VI were assessed using Cell Counting Kit-8, lactate dehydrogenase release and colony formation assays. The occurrence of ferroptosis was determined by assessing lipid peroxidation by reactive oxygen species, malondialdehyde levels, intracellular ferrous iron levels, and the mRNA and protein levels of glutathione peroxidase 4 (GPX4). The migratory and invasive abilities of HCC cells were examined using wound healing and Transwell assays. The results revealed that polyphyllin VI inhibited the proliferation, invasion and metastasis of HCC cells (HCCLM3 and Huh7 cells) by inducing ferroptosis. In addition, through a network pharmacology-based approach and molecular docking analyses, it was found that polyphyllin VI may target the signal transducer and activator of transcription 3 (STAT3). HCC cells were treated with polyphyllin VI or a STAT3 inhibitor (Stattic), both of which exerted similar inhibitory effects on protein expression. Furthermore, immunofluorescence staining revealed that polyphyllin VI significantly inhibited the nuclear translocation of p-STAT3 in HCC cells. Mechanistically, by the overexpression of STAT3, it was confirmed that STAT3 binds to GPX4 and promotes its protein expression and transcription, whereas polyphyllin VI induces ferroptosis by inhibiting the STAT3/GPX4 axis. Subsequently, *in vivo* experiments revealed that polyphyllin VI inhibited the growth of subcutaneously transplanted tumors. On the whole, findings of the present study suggest that polyphyllin VI inhibits STAT3 phosphorylation, which inhibits GPX4 expression and induces the ferroptosis of HCC cells, eventually inhibiting their invasion and metastasis. These data suggest that polyphyllin VI may be a candidate for the prevention and treatment of HCC.

Correspondence to: Professor Xiaozhou Zhou or Dr Zhiyi Han, Department of Liver Disease, Shenzhen Traditional Chinese Medicine Hospital, 1 Fuhua Road, Futian, Shenzhen, Guangdong 518033, P.R. China
E-mail: zxz1006@gzucm.edu.cn
E-mail: tcmhzy@hotmail.com

*Contributed equally

Key words: hepatocellular carcinoma, polyphyllin VI, ferroptosis, glutathione peroxidase 4, signal transducer and activator of transcription 3

Introduction

Primary liver cancer is the common cause of the global cancer burden, and 90% of primary liver cancer cases are hepatocellular carcinoma (HCC) (1). HCC ranks sixth in incidence among malignant tumors and third among cancer-related deaths (2). According to the 2020 global cancer statistics, the incidence and mortality rate associated with liver cancer in China ranked first worldwide (2). In recent years, with advancements being made in systemic therapy, non-surgical treatments for HCC have gradually emerged. An objective response rate of ~30% can be achieved using anti-angiogenic drugs combined with immunotherapy for the treatment of advanced or unresectable liver cancer (3). Although the efficacy of advanced HCC treatments has notably improved, serious challenges remain. It has been found that, during the clinical application of targeted drugs, some patients are susceptible to drug resistance and the median survival rate remains low (3). Therefore, the development of effective therapeutic drugs is mandatory in order to

provide patients with HCC with more treatment opportunities and improved survival benefits.

Ferroptosis is a newly discovered oxidative cell death characterized by cystine depletion or glutathione peroxidase 4 (GPX4) inactivation and the iron-dependent accumulation of lethal lipid peroxidation on the plasma membrane or elsewhere within the cell (4). Studies have confirmed that ferroptosis plays a critical regulatory role in the pathogenesis and treatment of cancers, including HCC, and is mainly suppressed in tumor cells to maintain survival (5). For example, ubiquitin-like modification activator 1 triggers the inhibition of ferroptosis by upregulating nuclear factor erythroid-2 related factor 2 (Nrf2) signaling and downregulating Fe^{2+} levels, promoting the development of HCC (6). Furthermore, sorafenib and sulfasalazine synergistically inhibit branched chain acid aminotransferase 2, which induces the ferroptosis of HepG2 cells (7). In addition, the inhibition of ADP-ribosylation factor 6 activates long-chain acyl-CoA synthetase 4, inducing ferroptosis, to overcome gemcitabine resistance in pancreatic cancer cells (8); this action also downregulates microRNA-522, promotes arachidonic acid 5 lipid oxygenase expression to induce ferroptosis, and enhances cisplatin/paclitaxel sensitivity in gastric cancer cells (9). These findings suggest that the induction of ferroptosis may present a novel therapeutic approach for HCC treatment.

Traditional Chinese medicine (TCM) involves the combination of the traditional culture and wisdom of the Chinese nation (10). TCM is characterized by less toxicity and fewer side-effects, more therapeutic targets and an enhanced efficacy (10). TCM contains numerous bioactive components, some of which exhibit activity against HCC (11). Therefore, identifying novel drugs for the treatment of HCC from TCM monomer compounds may be a practical approach. The authors screened a drug library of TCM monomers containing 1,444 compounds and identified polyphyllin VI as a potential therapeutic drug for HCC.

Polyphyllin VI (PPVI), an active saponin isolated from *Paris polyphylla*, has been shown to exert potent anticancer effects in a variety of malignant tumors. PPVI has been shown to induce non-small cell lung cancer (NSCLC) cell death through the induction of the NF-κB/NLR family pyrin domain containing 3/gasdermin D signaling axis (12), to exert anticancer effects against breast cancer cells by modulating RELT-like protein 2 (13), and to induce the apoptosis and autophagy of osteosarcoma through c-Jun N-terminal kinase (14). However, the effects of PPVI on HCC remain unclear. The present study investigated the therapeutic effects of PPVI on HCC and assessed the possible mechanisms through which these effects may be exerted.

Materials and methods

Reagents and antibodies. Traditional Chinese Medicine Library (cat. no. L8300), PPVI (cat. no. S9302), β-lapachone (cat. no. S7261), 3-methyladenine (3-MA, cat. no. S2767) inhibitors and Ac-DEVD-CHO (cat. no. S7901) were purchased from Selleck Chemicals; Stattic (cat. no. HY-13818) and ferrostatin-1 (Fer-1, cat. no. HY-100579) were purchased from MedChem Express. GPX4 (cat. no. ab125066), signal transducer and activator of transcription 3 (STAT3; cat. no. ab68153), phosphorylated (p-)STAT3 (pY705; cat. no. ab76315), N-cadherin (cat. no. ab18203), Vimentin (cat. no. ab92547), E-cadherin (cat. no. ab40772) and goat anti-rabbit IgG H&L (HRP; cat. no. ab6721) antibodies were purchased from Abcam. The GAPDH (2118S) antibody was purchased from Cell Signaling Technology, Inc. The goat anti-rabbit IgG (H+L) cross-adsorbed secondary antibody and cyanine3 (A-10520) were purchased from Invitrogen; Thermo Fisher Scientific, Inc.

Cell culture and treatment. The HCCLM3 cells were purchased from the China Center for Type Culture Collection (CCTCC), and the Huh7 cells were purchased from Suyan Biotechnology Co., Ltd. The THLE-2 cells were purchased from Meisen Cell Technology Co., Ltd. The HCCLM3 and Huh7 Cells were cultured in DMEM/high-glucose medium (Gibco; Thermo Fisher Scientific, Inc.) with 10% fetal bovine serum (FBS; Gibco; Thermo Fisher Scientific, Inc.) and 1% penicillin-streptomycin (Gibco; Thermo Fisher Scientific, Inc.) at 37˚C and 5% CO_2. The THLE-2 cells require a special coating medium (CTCC-002-30, Meisen Cell Technology Co., Ltd.) and were incubated overnight in an incubator at 37˚C and 5% CO_2 and cultured in BEGM™ BulletKit™ medium (cat. no. CC-3170, Lonza Group, Ltd.) with 10% FBS. The HCC cells were observed and representative images were captured under an inverted microscope (Ts2R-FL, Nikon Corporation; x100 magnification) at 0 and 24 h following drug intervention. The HCC cells were treated with PPVI (4 μM) at 37˚C for 24 h, following which different assays were performed. Inhibitors, such as 3-MA (1 mM), Ac-DEVD-CHO (50 μM) and Fer-1 (1 μM) for 2 h prior to treatment with PPVI (4 μM) for 24 h.

Transfection with overexpression plasmids. The plasmids that included PIRES2-EGFP (hSTAT3-IRES2-EGFP, oeSTAT3 and BW2486) and PIRES2-EGFP (No-Targeting Plasmid, the control plasmid and BVA15) were purchased from Hangzhou Youming Biotechnology Co., Ltd. For transfection, Lipofectamine 3000 transfection reagent (GlpBio) diluted in Opti-MEM (Gibco; Thermo Fisher Scientific, Inc.) was used (1:1 ratio; two tubes). After seeding, the cells were grown to 70-90% confluency and then transfected, with 5 μg/μl of the transfected DNA concentration. The DNA master mix was prepared by diluting DNA in Opti-MEM, then adding Lipofectamine 3000 reagent and mixing well. The diluted DNA was added to each tube of diluted Lipofectamine 3000 reagent and incubated for 10-15 min at room temperature. The DNA-lipid complex was added to the cells and incubated for 3 days at 37˚C.

Subcutaneous tumor model and drug administration. All animal experiments were approved (No. 20220070) by the Animal Ethics Committee (AEC) of the China Science and Technology Industry Holdings (Shenzhen) Co., Ltd. Male BALB/c nude mice (n=9), 4 weeks old, were purchased from the Guangdong Medical Laboratory Animal Center. All mice were housed under the following conditions: A 12-h light/dark cycle (lights on, 07:00; lights off, 19:00), a temperature of 22±2˚C and a humidity of 50±10%, and were provided with free access to standard chow and water. The Huh7 cells ($1x10^7$ in 0.1 ml DMEM) were injected subcutaneously into the right flanks of the nude mice. After 7 days, the mice were

randomly divided into three groups (three mice per group) as follows: The control group (0.9% NaCl/day), PPVI-treated group (PPVI at 10 mg/kg/day) and the group treated with PPVI (10 mg/kg/day) + Fer-1 (10 mg/kg/day). The weight of the tumors and tumor size were measured daily. Following the intraperitoneal administration of the treatments for 10 consecutive days, the mice were sacrificed, and the serum was used to measure alanine transaminase (ALT, cat. no. C009-2-1) and aspartate aminotransferase (AST, cat. no. C010-2-1) (both from Jiancheng Bioengineering Institute) levels. The mice were euthanized by an intraperitoneal injection of pentobarbital sodium (200 mg/kg). Blood was then obtained from the orbital sinus, and the livers and subcutaneous tumors were removed. During the animal experiments, the maximum diameter of the tumors was measured daily. When the longest diameter of a single tumor was 20 mm, the experiment was terminated and the animals were euthanized. Following euthanasia, the death of the animal was confirmed by documenting the disappearance of the pain response (i.e., unresponsiveness to toe compressions with hands or forceps) and the observation of cardiac arrest and apnea. Liver and tumor tissues were collected for detection using hematoxylin and eosin (H&E) staining and immunohistochemistry, as described below.

Cell counting kit-8 (CCK-8) assay. The HCC cells were treated with the indicated concentrations of PPVI (from 1 to 10 μM) or Stattic (6 μM) for 24 h. The HCC cells were then treated with or without 3-MA (1 mM), Ac-DEVD-CHO (50 μM) and Fer-1 (1 μM) inhibitors for 2 h prior to treatment with PPVI for 24 h. Cell viability was assessed using a CCK-8 assay (cat. no. C0043, Beyotime Institute of Biotechnology). The optical density (OD) value of the sample was obtained at 450 nm using a microplate reader (BioTek Instruments, Inc.).

Cell cloning assay. After the HCCLM3 or Huh7 cells were seeded in six-well plates at a density of 800 cells/well, they were subjected to PPVI (2, 4, 6, 8 and 10 μM) or PPVI (4 μM) with Fer-1 (1 μM). The medium was replaced for 3 days and the cells were cultured until the number of monoclonal cells was >50. The cells were fixed with 4% paraformaldehyde at 25˚C for 30 min, stained with crystal violet (cat. no. BL802A, Biosharp Life Sciences) for 30 min at 25˚C, and photographed using a digital camera (Ts2R-FL, Nikon Corporation).

Lactate dehydrogenase (LDH) cytotoxicity assay. The HCCLM3 or Huh7 cells were treated with or without 3-MA (1 mM), Ac-DEVD-CHO (50 μM) and Fer-1 (1 μM) inhibitors for 2 h prior to treatment with PPVI (4 μM) for 24 h. Following the instructions provided with the LDH Cytotoxicity Detection Kit (Beyotime Institute of Biotechnology), the plates were incubated at 37˚C for 30 min in the dark. The OD values at 490 nm were obtained using a microplate reader (BioTek Instruments, Inc.).

Cell wound healing assay. The HCCLM3 and Huh7 cells were seeded in a six-well plate at a density of $4x10^5$ cells/well. When the cell density reached 90% confluency, the confluent cell monolayer was scraped using a pipette tip. The cells were incubated in serum-free medium as designed for the experiments. Images of the same scratched area at 0 and 24 h were captured (Ts2R-FL, Nikon Corporation).

Transwell invasion assay. The cells were starved and incubated for 12 h in advance, and $2.5x10^5$ HCC cells were seeded in the upper chamber (cat. no. 3422, Corning, Inc.) of the Transwell, followed by PPVI (4 μM) or PPVI (4 μM) + Fer-1 (1 μM) for 24 h. The lower chamber contained DMEM with 20% FBS. Following incubation of the Transwell plate at 37˚C for 24 h, the invaded cells were fixed with formaldehyde for 30 min at 25˚C and stained with crystal violet (cat. no. BL802A, Biosharp Life Sciences) for 30 min at 25˚C. Finally, the invaded cells were observed and photographed under an inverted microscope (Nikon, Ts2R-FL).

Transmission electron microscopy (TEM). After the HCCLM3 and Huh7 cells were treated with PPVI (4 μM) and incubated for 24 h at 37˚C, the cells were collected by centrifugation (3,000 x g, 2 min, 37˚C), supplemented with 2.5% Gluta fixative (Beijing Solarbio Science & Technology Co., Ltd.) at 4˚C for 48 h. The cells were then dehydrated in a graded ethanol series, infiltrated with propylene oxide, embedded in an epoxy resin (cat. no. 10000418, SPI Supplies) at 37˚C for 12 h and sectioned to a thickness of 70 nm. åSubsequently, the ultrathin sections were observed and photographed using an HT7800 transmission electron microscope (Hitachi, Ltd.).

Mitochondrial membrane potential detection (JC-1). The HCCLM3 or Huh7 cells were seeded in six-well plates, and treated with PPVI (2, 4 and 6 μM) or PPVI (4 μM) with Fer-1 (1 μM) for 24 h. The JC-1 fluorescent probe (Beyotime Institute of Biotechnology) was then added according to the instructions of the manufacturer to observe the mitochondrial membrane potential (MMP) changes under a fluorescence microscope (DMIL4000, Leica Microsystems, Inc.).

Glutathione (GSH) detection. Following 24 h of treatment with PPVI (2, 4 and 6 μM) or PPVI (4 μM) with or without Fer-1 (1 μM), the working solution was added according to the instructions provided with the GSH assay kit (cat. no. S0053, Beyotime Institute of Biotechnology) using a single-point assay, and absorbance was measured using a microplate reader (BioTek Instruments, Inc.) after 25 min.

Malondialdehyde (MDA) detection. The HCCLM3 or Huh7 cells were homogenized in MDA lysis buffer, and centrifuged at 13,000 x g for 10 min at 4˚C to obtain 200 μl supernatant. The MDA assay kit (cat. no. MAK085, MilliporeSigma) was used to detect the MDA content. Finally, the absorbance value was measured at 532 nm using a microplate reader (BioTek Instruments, Inc.).

Iron content determination. The HCCLM3 or Huh7 cells were treated with PPVI (2, 4 and 6 μM) or PPVI (4 μM) with Fer-1 (1 μM) for 24 h, and the Fe^{2+} levels were determined according to the instructions provided with the iron assay kit (cat. no. MAK025, MilliporeSigma).

Divalent iron on probe detection. FerroOrange fluorescent probes (Dojindo Laboratories, Inc.) were loaded in the HCC cells following 24 h of PPVI (2, 4 and 6 μM) or PPVI (4 μM) with or without Fer-1 (1 μM). According to the instructions provided by the manufacturer, following 30 min at 37˚C of incubation, the changes in the Fe^{2+} content were observed and

photographed using a fluorescence microscope (Ts2R-FL, Nikon Corporation).

Active oxygen determination. Intracellular superoxide anion levels were determined using dihydroethidium (DHE; Beyotime Institute of Biotechnology). Following the manufacturer's instructions, a DHE solution was incubated with the cells at 37˚C for 30 min and the cells were then observed and photographed under a fluorescence microscope (Ts2R-FL, Nikon Corporation).

Western blot analysis. The cells were lysed and homogenized using RIPA lysis buffer (cat. no. 89900, Thermo Fisher Scientific, Inc.), and the protein concentration was detected using a BCA assay kit (cat. no. 23227, Thermo Fisher Scientific, Inc.). The proteins were separated by SDS-PAGE (10% gels) and transferred onto PVDF membranes. After the membranes were incubated with 5% skim milk at 25˚C for 1 h, they were incubated with the corresponding primary antibodies (1:1,000; all antibodies used are listed above in the Reagents and antibodies section) at 4˚C overnight, followed by incubation with the secondary antibody (1:2,000) for 1 h at 25˚C. The bands were detected using a chemiluminescent HRP substrate (WBKLS0500, MilliporeSigma) and visualized with the ChemiDoc XRS system (Bio-Rad Laboratories, Inc.). Densitometric analysis of the western blots was performed using ImageJ V1.8.0 (National Institutes of Health, Inc.).

Immunofluorescence staining. The HCC cells were treated with PPVI (2, 4 and 6 μM) or PPVI (4 μM) with or without Fer-1 (1 μM) and incubated for 24 h at 37˚C. The cells were fixed with 4% polyformaldehyde, permeabilized with 0.5% Triton X-100 (T9284, MilliporeSigma), blocked with 5% goat serum (BL210A, Biosharp Life Sciences) and incubated overnight with the required amount of primary antibody such as GPX4, N-cadherin, Vimentin and E-cadherin (1:200) in a humidified box at 4˚C. The cells were incubated with the goat anti-rabbit IgG (H+L) antibody, Cy3 (1:200) at 25˚C for 1 h in the dark. Nuclear DAPI (BL105A, Biosharp Life Sciences) was used for counterstaining for 15 min at 25˚C in the dark with antifade mounting medium (P0126, Beyotime Institute of Biotechnology) to mount the slides and the slides were then photographed (Ts2R-FL, Nikon Corporation). The procedure was repeated with the Huh7 cells.

RNA isolation and reverse transcription-quantitative PCR (RT-qPCR). Total RNA was extracted from the HCC cells using the AG RNAex isolation system (Accurate Biotechnology Co., Ltd.) according to the manufacturer's protocol. Complementary DNA was synthesized using reverse transcription kits (cat. no. AG11728, Jiangsu Accuracy Biotechnology Co., Ltd.). qPCR was performed using a QuantStudio5 system (Thermo Fisher Scientific, Inc.) with SYBR-Green (cat. no. AG11718, Jiangsu Accuracy Biotechnology Co., Ltd.) and the thermocycling conditions were as follows: 95˚C for 30 sec, 95˚C for 5 sec and 60˚C for 30 sec, for 40 cycles. The $2^{-\Delta\Delta Cq}$ method was used to analyze the RT-qPCR data (15). The sequences of the primers used are as follows: GPX4 forward, 5'-CCCGATACG CTGAGTGTGGTTTG-3' and reverse, 5'-CCTTGCCCTTGG GTTGGATCTTC-3'; STAT3 forward, 5'-TGTGATGCTTCC CTGATTGTGACTG-3' and reverse, 5'-TCGCTTGGTGGT GGAGGAGAAC-3'; and GAPDH forward, 5'-CAAGGCTGT GGGCAAGGTCATC-3' and reverse, 5'-GTGTCGCTGTTG AAGTCAGAGGAG-3'.

Immunohistochemistry. The tissues were paraffin-embedded, sectioned, dewaxed in xylene, soaked in 100 to 70% gradient ethanol and placed in PBS. Citric acid retrieval solution (cat. no. P0086, Beyotime Institute of Biotechnology) was then added, and the slices were placed in the microwave for 20 min at 100˚C and then rinsed with PBS three times, for 5 min each. After washing, 5% blocking serum was added in a dropwise manner for blocking for 30 min at 37˚C, and primary antibody such as p-STAT3, STAT3, GPX4 (1:200) with 5% BSA was then added in a dropwise manner for overnight incubation at 4˚C. The following day, MaxVision™ HRP-Polymer anti-mouse/rabbit IHC kit (cat. no. KIT-5020, MXB Biotechnologies) was added 50 μl followed by incubation at 25˚C for 15 min. Subsequently, 50 μl developer diaminobenzidine working solution (cat. no. DAB-0031, MXB Biotechnology Co., Ltd.) was added followed by incubation at room temperature for 3 min. The sections were counterstained with hematoxylin for 40 sec at 25˚C, dehydrated, mounted, and observed under a microscope (Axio Imager M2, Zeiss AG).

Network pharmacology-based and molecular docking analyses. The human targets of PPVI were obtained from the SwissTarget prediction database (http://swisstargetprediction.ch/), and the DrugBank (https://www.drugbank.ca/), GeneCards (https://www.genecards.org/), DisGeNET (http://www.disgenet.org/home), Online Mendelian Inheritance in Man (OMIM, https://www.omim.org/), TTD (http://db.idrblab.net/ttd) and PharmGKB databases (https://www.pharmgkb.org/) were then searched using the key words 'liver cancer' and 'liver carcinoma'. All obtained targets were merged and duplicate targets were removed. The targets of PPVI were used to intersect with the targets of liver cancer to obtain the anti-liver cancer targets of PPVI. The data were uploaded to the STRING 11.5 database to obtain protein-protein interaction (PPI) information and analyzed using Cytoscape 3.9.1 (https://cytoscape.org/). Cytoscape was used to calculate network topology parameters, including degree centrality, closeness centrality, betweenness centrality, and clustering coefficient. Finally, AutoDock 4.2.6 (https://autodock.scripps.edu/) was used to perform molecular docking between PPVI and key targets, and PyMOL (https://pymol.org/2/) was used to obtain a visual 2D map.

Statistical analysis. All experiments were repeated independently at least three times. GraphPad Prism 9.4 software (GraphPad Software, Inc.) was used for data analysis using an unpaired t-test and one-way ANOVA (with Tukey's multiple comparisons test). A value of $P<0.05$ was considered to indicate a statistically significant difference.

Results

Identification of compounds that can induce cell death in HCC cells using high-throughput screening. To identify compounds with therapeutic efficacy in HCC, a pilot library was screened which comprised ~1,444 TCM monomeric

representative compounds with an ability to inhibit cell activity in HCCLM3 cells at a concentration of 10 μM. The screening process followed in the present study is illustrated in Fig. 1A. The HCCLM3 cells were treated with 1,444 monomers for 24 h and cell viability was then examined. As shown in Fig. 1B, 20 compounds (Fig. S1A and B) inhibited the growth of the HCCLM3 cells by <30%. Subsequently, the Huh7 cells were treated with these monomers 10 μM for 24 h, and a second screening was performed using CCK-8 assay (Fig. 1C). The Venn diagram shown in Fig. 1D illustrates the screening process, demonstrating monomeric molecules with toxic effects in both HCCLM3 and Huh7 cells. The intersection of the Venn diagram indicates two compounds, PPVI and β-lapachone. The Huh7 cells were then treated with PPVI and β-lapachone (10 μM) for 24 h, which was found to exert potent cytotoxic effects on both cell lines (Fig. 1E). The further comparison of the inhibitory effects of PPVI and β-lapachone on HCC cell (HCCLM3 and Huh7 cells) viability revealed that PPVI exerted the most pronounced inhibitory effect on the viability of HCC cells (Fig. 1E). The chemical structural formula of PPVI is presented in Fig. 1F.

To further analyze the cytotoxic effects of PPVI on HCC cells, the cells were treated with various concentrations of PPVI. The results revealed that PPVI inhibited the viability of HCCLM3 and Huh7 cells in a concentration-dependent manner (Fig. 1G and H). Compared with the normal liver cells (THLE-2), PPVI (4 μM) also exerted a significant inhibitory effect on HCC cell viability (Fig. 1I). The light microscopy images demonstrated that cell contraction and cell death increased with the increasing concentrations of PPVI (Fig. 1J and K). Cell cloning experiments also revealed that the proliferative capacities of the HCCLM3 and Huh7 cells were negatively associated with the concentration of PPVI (Fig. 1L and M).

Ferroptosis contributes to the cytotoxic effects of PPVI on HCC cells. The present study then examined the morphology of the treated cells in order to explore the mechanisms underlying PPVI-induced cell death. TEM analysis revealed that the HCCLM3 and Huh7 cells treated with PPVI (4 μM) for 24 h exhibited a decrease in mitochondrial volume, an increase in bilayer membrane density, and a decrease or disappearance of mitochondrial cristae (Fig. 2A and B), which are typical morphological features of ferroptosis. To verify whether this form of cell death involved ferroptosis, the HCCLM3 and Huh7 cells were treated with PPVI in the absence or presence of several cell death inhibitors. Combination treatment with the autophagy inhibitor, 3-MA, and the pyroptosis inhibitor, Ac-DEVD-CHO, did not prevent the death of the cells treated with PPVI (Fig. 2C-F), and the ferroptosis inhibitor, Fer-1, exerted the most pronounced reversal effect (Fig. 2C and D). Apoptosis or necrosis can cause damage to the cell membrane structure, and the quantitative analysis of cytotoxicity was achieved by detecting the activity of LDH released from the cells with plasma membrane rupture (Fig. 2E and F). Furthermore, in the fluorescence images of JC-1-stained mitochondria (Fig. 2G and H), red fluorescence representing an intact MMP was observed in the control group and a low MMP was observed in the PPVI-treated groups (2, 4 and 6 μM) with increasing concentrations.

PPVI-induced ferroptosis in HCC cells. To explore whether ferroptosis is a key determinant of HCC cell death induced by PPVI, several ferroptosis events were examined in HCC cells, including ROS accumulation, GSH, MDA, the Fe^{2+} content and GPX4 expression. GSH levels in the HCCLM3 and Huh7 cells were found to gradually decreased with the increasing concentrations of PPVI (2, 4 and 6 μM) (Fig. 3A and B). However, PPVI upregulated the MDA levels in a concentration-dependent manner (Fig. 3C and D). In addition, the intracellular Fe^{2+} levels significantly increased upon stimulation with 4 and 6 μM PPVI (Fig. 3E and F). Consistently, when the Fe^{2+} content was detected using a FerroOrange fluorescent probe, the accumulation of Fe^{2+} in the cells was promoted by the increase in the PPVI concentration (Fig. 3G). The level of cellular ROS was then detected using DHE. As the concentration of PPVI increased, the red fluorescence in the HCC cells was enhanced, indicating that the intracellular ROS level was positively associated with the concentration of PPVI, which suggested that PPVI induced oxidative stress in the HCC cells (Fig. 3H). The results also revealed that the GPX4 protein expression levels in the HCCLM3 and Huh7 cells were negatively associated with the concentration of PPVI (Fig. 3I and J).

The ferroptosis inhibitor, Fer-1, attenuates PPVI-induced cell death by inhibiting the ferroptosis of HCC cells. To further investigate the association between mitochondrial damage and ferroptosis induced by PPVI, the ferroptosis inhibitor, Fer-1, was used. Mitochondrial fluorescence staining was performed using HCC cells treated with PPVI + Fer-1, and an increase in aggregate JC-1 and a decrease in monomeric JC-1 were observed compared to the PPVI group (Fig. 4A and B), suggesting that Fer-1 can alleviated mitochondrial damage induced by PPVI. Changes in the intracellular levels of GSH, MDA and Fe^{2+} were also examined following co-treatment with PPVI and Fer-1. Consistently, GSH expression increased in the PPVI + Fer-1 group compared with that in the PPVI group (Fig. 4C and D), whereas the contents of MDA and Fe^{2+} decreased in the PPVI + Fer-1 group (Fig. 4E-H). Furthermore, the levels of ROS and ferrous iron were decreased in the PPVI + Fer-1 group compared with the PPVI group (Fig. 4I and J). Moreover, the protein expression levels of GPX4 were measured following co-treatment with PPVI and Fer-1 using western blot analysis. Compared with the PPVI group, the protein expression level of GPX4 in the PPVI + Fer-1 group was higher (Fig. 4K and L). An analysis of the GPX4 mRNA levels also revealed that its expression was reduced by PPVI, whereas it was increased in the PPVI + Fer-1 group (Fig. 4M). These results suggest that Fer-1 reverses PPVI-induced mitochondrial damage and the ferroptosis of HCC cells.

PPVI inhibits HCC cell invasion and migration by inducing ferroptosis. The present study then examined the effects of PPVI on the invasion and migration of HCC cells. Following treatment of the HCCLM3 and Huh7 cells with PPVI or PPVI combined with Fer-1, the PPVI + Fer-1 combination exhibited a lower ability to inhibit colony formation than PPVI alone, indicating that Fer-1 reversed cell death induced by PPVI (Fig. 5A and B). The wound healing assay revealed that PPVI markedly inhibited the wound-healing ability of the HCC cells

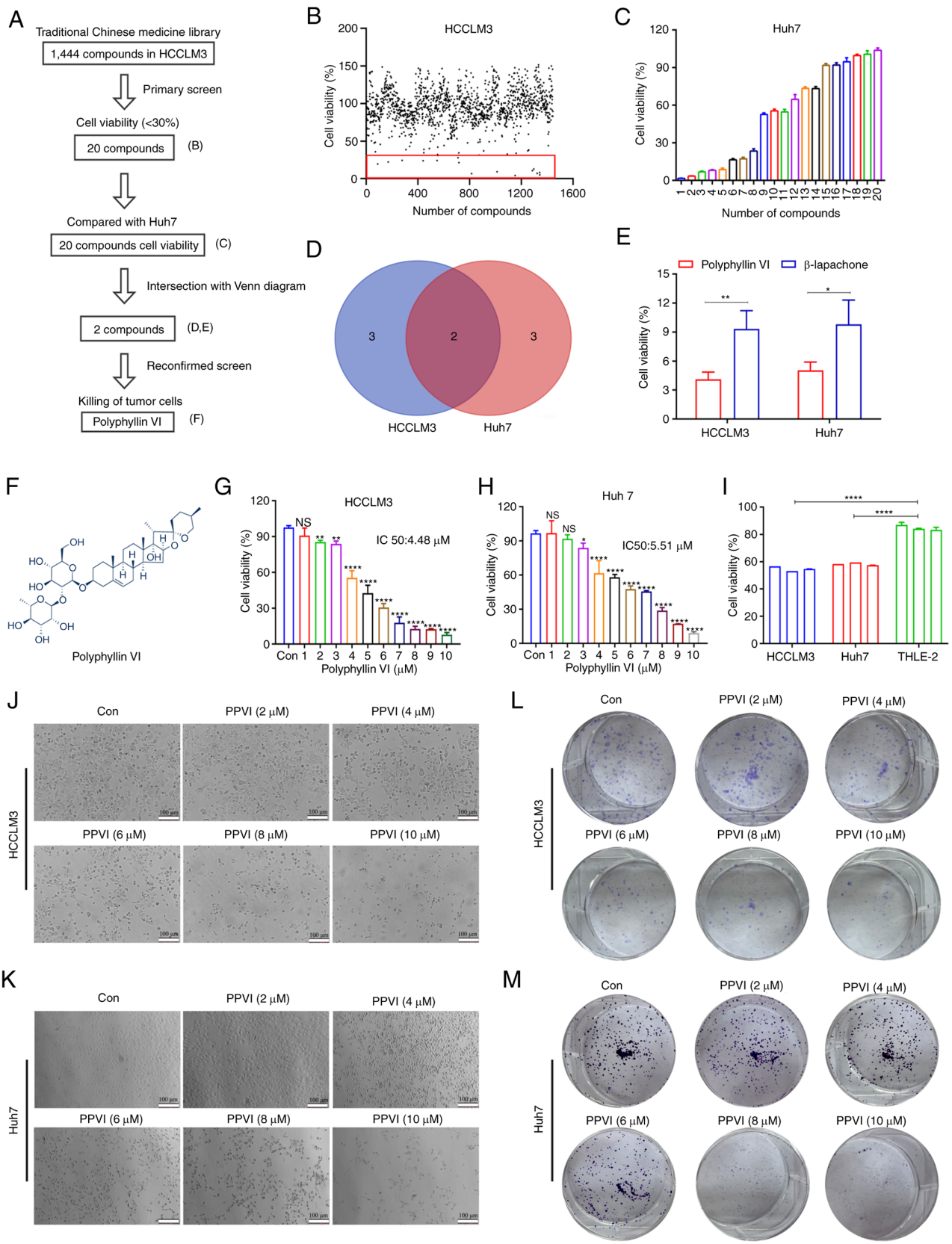

Figure 1. Identification of compounds that can induce the death of hepatocellular carcinoma cells using high-throughput screening. (A) Flow chart of the high-throughput screening of 1,444 TCM monomer compounds. (B) Viability of HCCLM3 cells exposed to the drug candidate library. Each point represents the percentage of cell viability following treatment with the compounds at a concentration of 10 μM. The dots located in the red box indicate cell viability of <30%. (C) Viability of the Huh7 cells exposed to 20 compounds (Fig. S1A and B). (D) The Venn diagram intersection method was used to obtain a TCM monomer which exerts potent cytotoxic effects on HCCLM3 and Huh7 cells. (E) Viability of HCCLM3 and Huh7 cells exposed to PPVI and β-lapachone. (F) Chemical structure of PPVI. (G and H) Viability of HCCLM3 and Huh7 cells treated with increasing concentrations of PPVI. (I) Viability of hepatocellular carcinoma and THLE-2 cells treated with 4 μM PPVI. (J and K) Morphology of HCCLM3 and Huh7 cells following 24 h of treatment with increasing concentrations of PPVI; scale bars, 100 μm. (L and M) Colony formation of cells treated with various concentrations of PPVI. *P<0.05, **P<0.01 and ****P<0.0001 vs. control. NS, not significant; Con, control; TCM, traditional Chinese medicine; PPVI, polyphyllin VI.

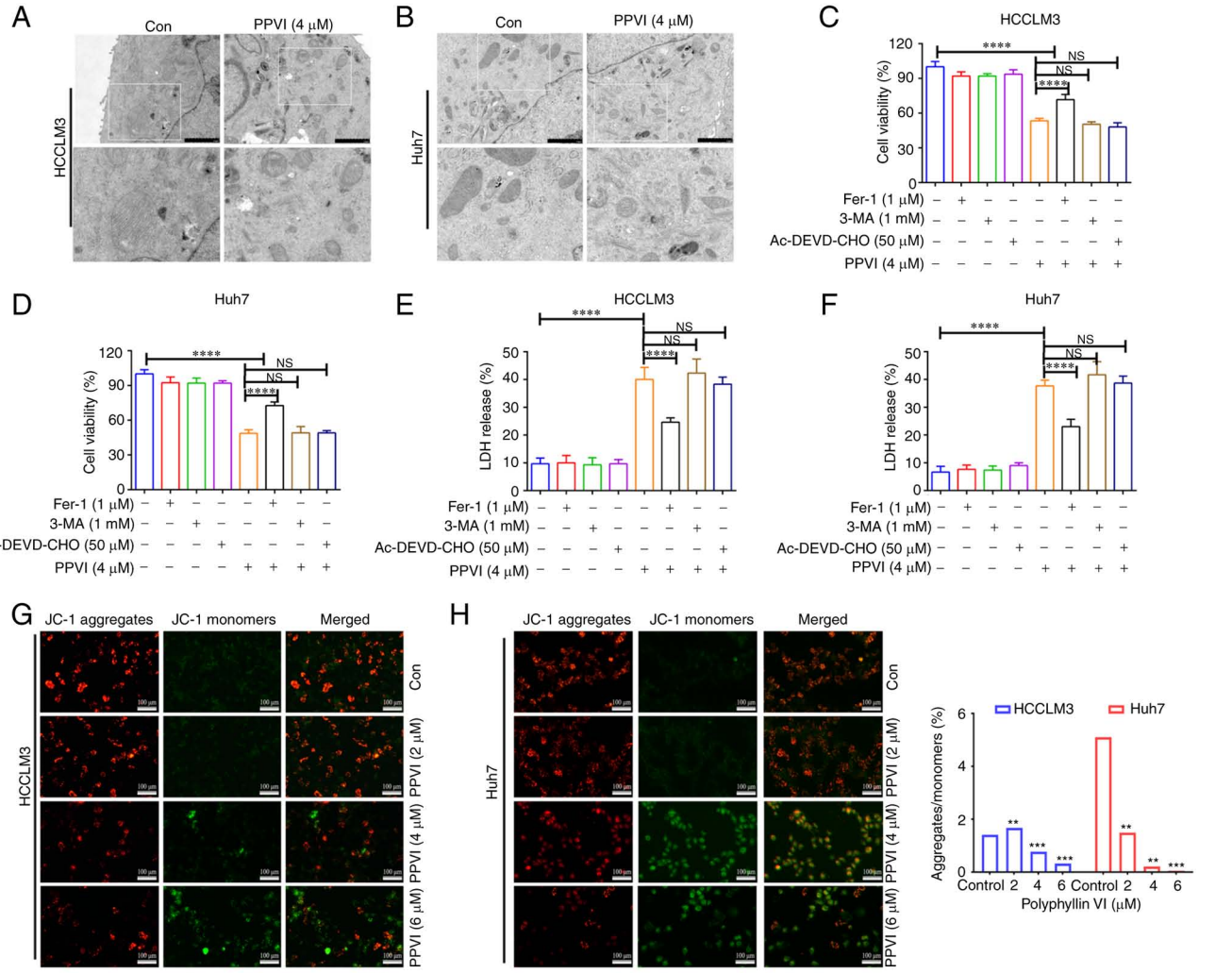

Figure 2. Ferroptosis contributes to the inhibition of the growth of hepatocellular carcinoma cells treated with polyphyllin VI. (A and B) Representative transmission electron microscopy images of HCCLM3 and Huh7 cells treated with the indicated concentrations of PPVI for 24 h. HCCLM3 and Huh7 cells were treated with or without 3-MA, Ac-DEVD-CHO and Fer-1 inhibitors for 2 h prior to treatment with PPVI for 24 h, and then subjected to different assays. (C and D) Analysis of cell viability. (E and F) Results of LDH assay. (G and H) Changes in the MMP of HCCLM3 and Huh7 cells treated with increasing PPVI concentrations were observed by detection with JC-1. Red fluorescence indicates a high MMP, whereas green fluorescence indicates a low MMP. **P<0.01, ***P<0.001 and ****P<0.0001 vs. control. NS, not significant; Con, control; MMP: mitochondrial membrane potential; PPVI, polyphyllin VI; Fer-1, ferrostatin-1; 3-MA, 3-methyladenine.

compared with the control group, whereas the PPVI-induced inhibition of the wound healing ability was markedly reversed by Fer-1 (Fig. 5C and D). Transwell assays revealed that PPVI markedly inhibited the number of invasive and migratory cells, and Fer-1 reversed this motility of the cells (Fig. 5E and F). As epithelial-mesenchymal transition (EMT) is one of the most critical mechanisms involved in cell migration and invasion, the effects of PPVI on the progression of EMT were investigated. The protein expression levels of E-cadherin, N-cadherin and Vimentin were examined using western blot analysis. The results revealed that PPVI increased the protein expression levels of E-cadherin in the HCCLM3 and Huh7 cells, whereas the levels of N-cadherin and Vimentin were decreased (Fig. 5G and H). The protein expression levels of E-cadherin were decreased in the PPVI + Fer-1 group, and the expression of N-cadherin and Vimentin was increased compared with that in the PPVI group (Fig. 5G and H). The results of immunofluorescence staining also revealed a similar result as those obtained for protein expression (Fig. 5I and J). These results thus suggest that PPVI inhibits the invasion and migration of HCC cells induced by the EMT mechanism.

PPVI inhibits the STAT3/GPX4 pathway in HCC cells. To examine the mechanisms by which PPVI induces the ferroptosis of HCC cells, a network pharmacology-based strategy was used to obtain PPVI targets in HCC by taking the intersection of the utility targets of PPVI and the targets in liver cancer. These target proteins were analyzed using a PPI network to obtain 42 nodes and 400 edges (Fig. 6A). The target proteins in the PPI network were then selected according to the criteria of degree ≥24, betweenness centrality ≥0.011, and closeness centrality ≥0.707, and nine core target proteins were finally identified, namely PIK3CA, JUN, FGF2, VEGFA, MTOR, CASP3, SRC, TNF and STAT3 (Fig. 6A). PPVI was molecularly docked with the aforementioned target proteins, and the binding energy data indicated that PPVI had a strong binding activity with STAT3 protein (Fig. 6B).

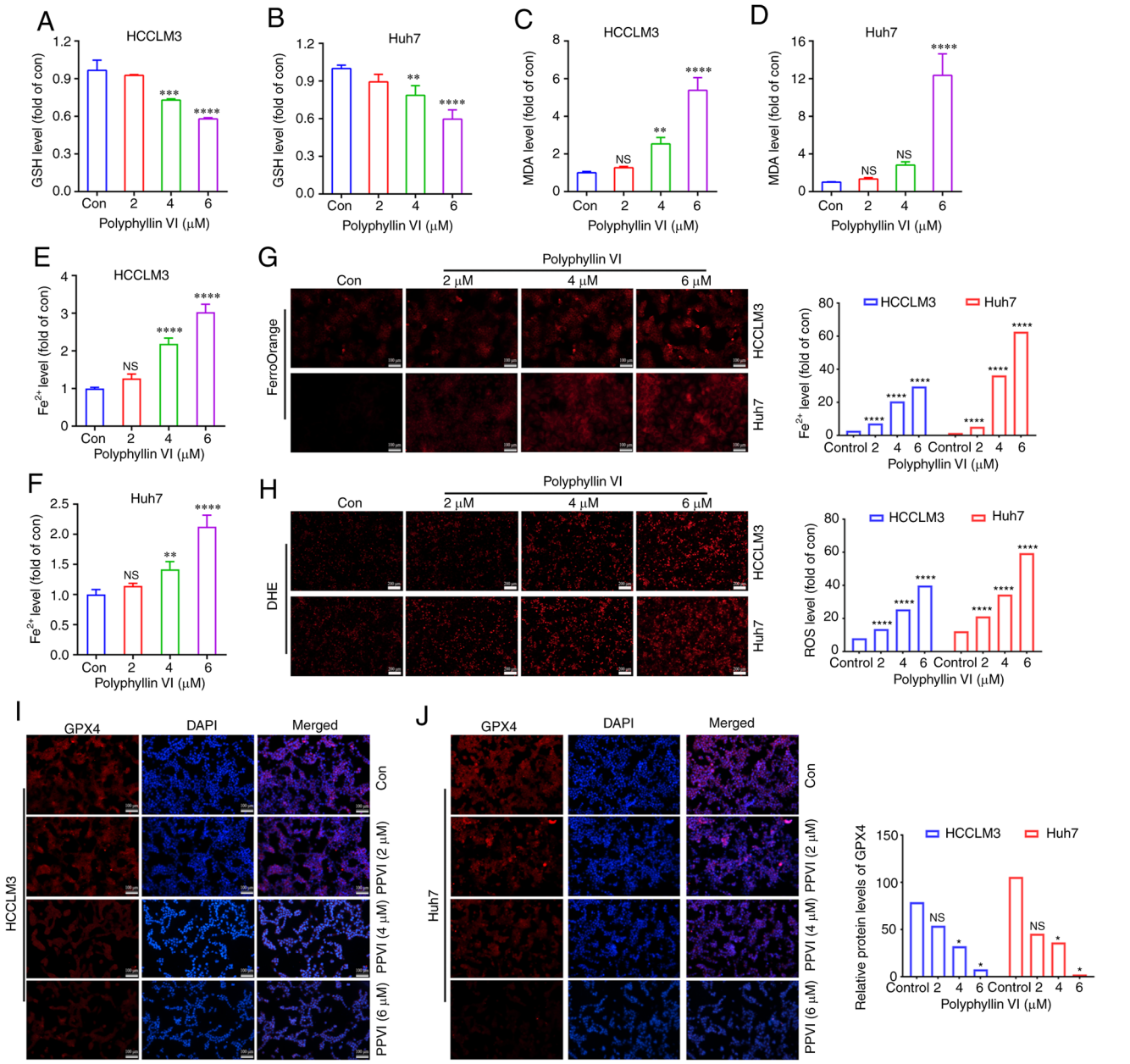

Figure 3. PPVI induces the ferroptosis of hepatocellular carcinoma cells. The HCCLM3 and Huh7 cells were treated with PPVI (2, 4 and 6 μM) for 24 h. (A and B) GSH levels in HCCLM3 and Huh7 cells. (C and D) MDA level detection. (E and F) Fe^{2+} level detection. (G) The Fe^{2+} content in HCCLM3 and Huh7 cells was detected using the FerroOrange fluorescent probe. (H) ROS levels in HCCLM3 and Huh7 cells were observed using DHE. (I and J) The protein expression levels of GPX4 in HCCLM3 and Huh7 cells were detected using immunofluorescence. *P<0.05, **P<0.01, ***P<0.001 and ****P<0.0001 vs. control. NS, not significant; Con, control; PPVI, polyphyllin VI; GSH, glutathione; MDA, malondialdehyde; DHE, dihydroethidium; ROS, reactive oxygen species; GPX4, glutathione peroxidase 4.

The present study then examined whether STAT3 inhibition promoted the ferroptosis of HCC cells. The HCCLM3 and Huh7 cells were treated with 4 μM PPVI and STAT3 inhibitor (6 μM Stattic), respectively. The results of western blot analysis revealed that PPVI significantly inhibited STAT3 and GPX4 protein expression, and the phosphorylation also decreased accordingly, which followed the downward trend induced by Stattic (Fig. 6C-E). Notably, the levels of ROS, ferrous iron, MDA and GSH, and GPX4 protein expression (based on western blot analysis) also exhibited similar changes in the cells treated with PPVI or Stattic compared with the control group (Fig. S2). Moreover, the wound healing assay revealed that PPVI or Stattic inhibited the wound healing ability of the HCC cells (Fig. S1C). Furthermore, the results of immunofluorescence staining indicated that the nuclear translocation of p-STAT3 in the HCC cells was suppressed with the increasing PPVI concentrations (Fig. 6F and G). These results suggest that PPVI may regulate the protein expression of the GPX4 through STAT3. Subsequently, to investigate the mechanisms through which STAT3 regulates GPX4, STAT3 was overexpressed in the HCCLM3 and Huh7 cells, and it was confirmed that STAT3 increased the GPX4 protein and mRNA levels (Fig. 6H-J).

PPVI induces ferroptosis by inhibiting the STAT3/GPX4 axis in HCC cells. The present study then examined whether PPVI induces ferroptosis by regulating the STAT3/GPX4 axis in HCC

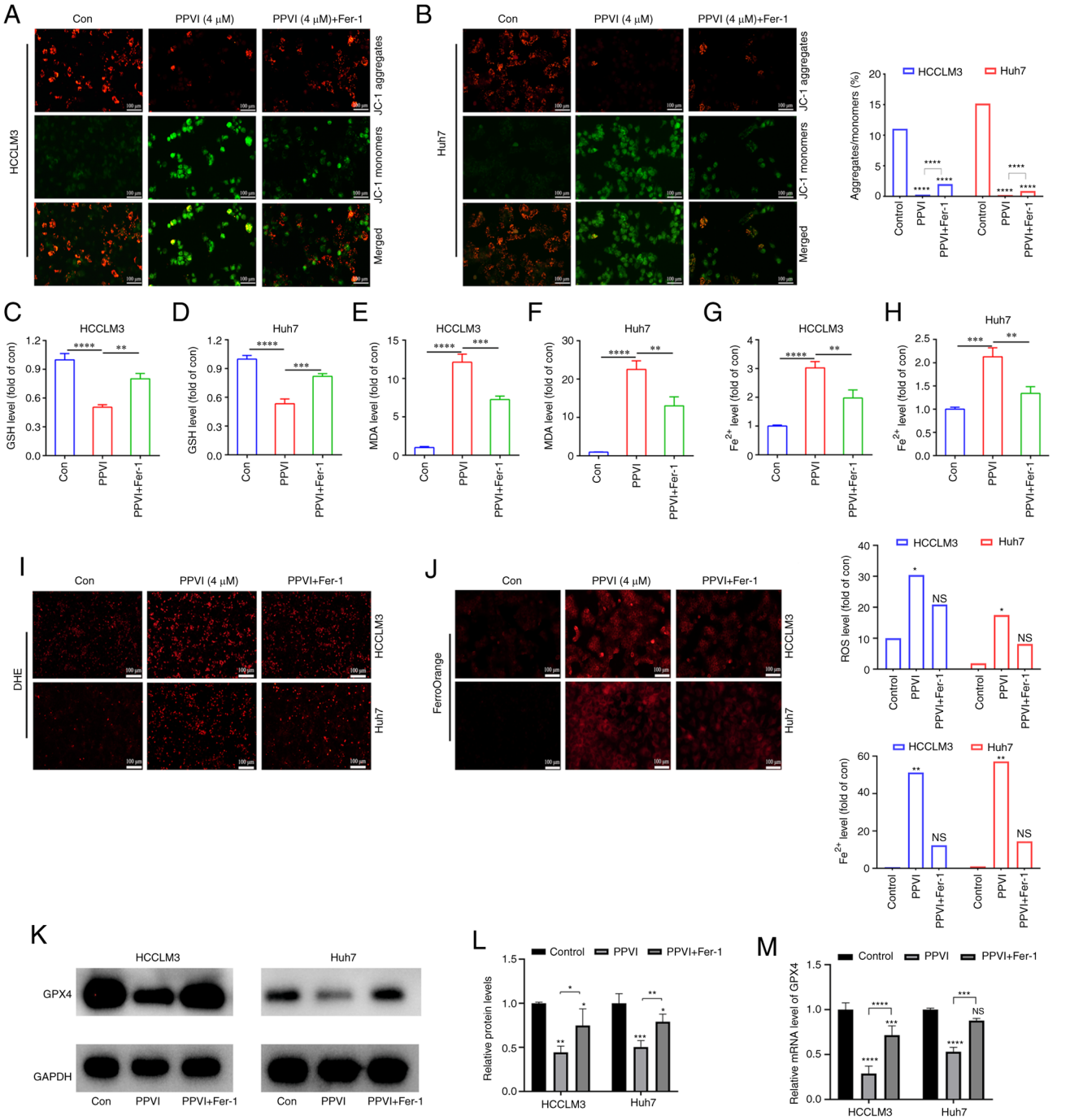

Figure 4. The ferroptosis inhibitor, Fer-1, attenuates polyphyllin VI-induced cell death by inhibiting the ferroptosis of HCC cells. The HCCLM3 and Huh7 cells were treated with or without Fer-1 for 2 h prior to treatment with PPVI for 24 h, after which different assays were performed. (A and B) Changes in the MMP of HCCLM3 and Huh7 cells were observed by MMP detection with JC-1. (C and D) GSH level detection in HCCLM3 and Huh7 cells. (E and F) MDA level detection in HCCLM3 and Huh7 cells. (G and H) Fe^{2+} levels in HCCLM3 and Huh7 cells. (I) ROS level detection in HCC cells observed using DHE. (J) Fe^{2+} level detection in HCCLM3 and Huh7 cells detected using FerroOrange fluorescent probe. (K and L) Western blot analysis of GPX4 in HCCLM3 and Huh7 cells. (M) Relative mRNA expression of GPX4 in HCC cells. *P<0.05, **P<0.01, ***P<0.001 and ****P<0.0001 vs. control or as indicated. NS, not significant; Con, control; HCC, hepatocellular carcinoma; PPVI, polyphyllin VI; MMP, mitochondrial membrane potential; DHE, dihydroethidium; ROS, reactive oxygen species; GPX4, glutathione peroxidase 4; Fer-1, ferrostatin-1.

cells. For this purpose, five groups were created, including one control group with nothing added. To reduce the influence of plasmid vectors on the experiment, an unloaded plasmid group and an unloaded plasmid + PPVI group were utilized. The remaining two groups were the overexpression STAT3 group and the overexpression STAT3 + PPVI group. After the HCC cells that overexpressed STAT3 were treated with 4 μM PPVI for 24 h, ROS and ferrous iron in the NT-Plasmid + PPVI group increased significantly; however, this effect was inhibited by STAT3 overexpression (Fig. 7A and B). Furthermore, the increase in MDA and the decrease in GSH levels induced by PPVI were also reversed by STAT3 overexpression (Fig. 7C and D). In addition, the PPVI-induced decrease in GPX4 expression was partially reversed by STAT3 overexpression (Fig. 7E and F).

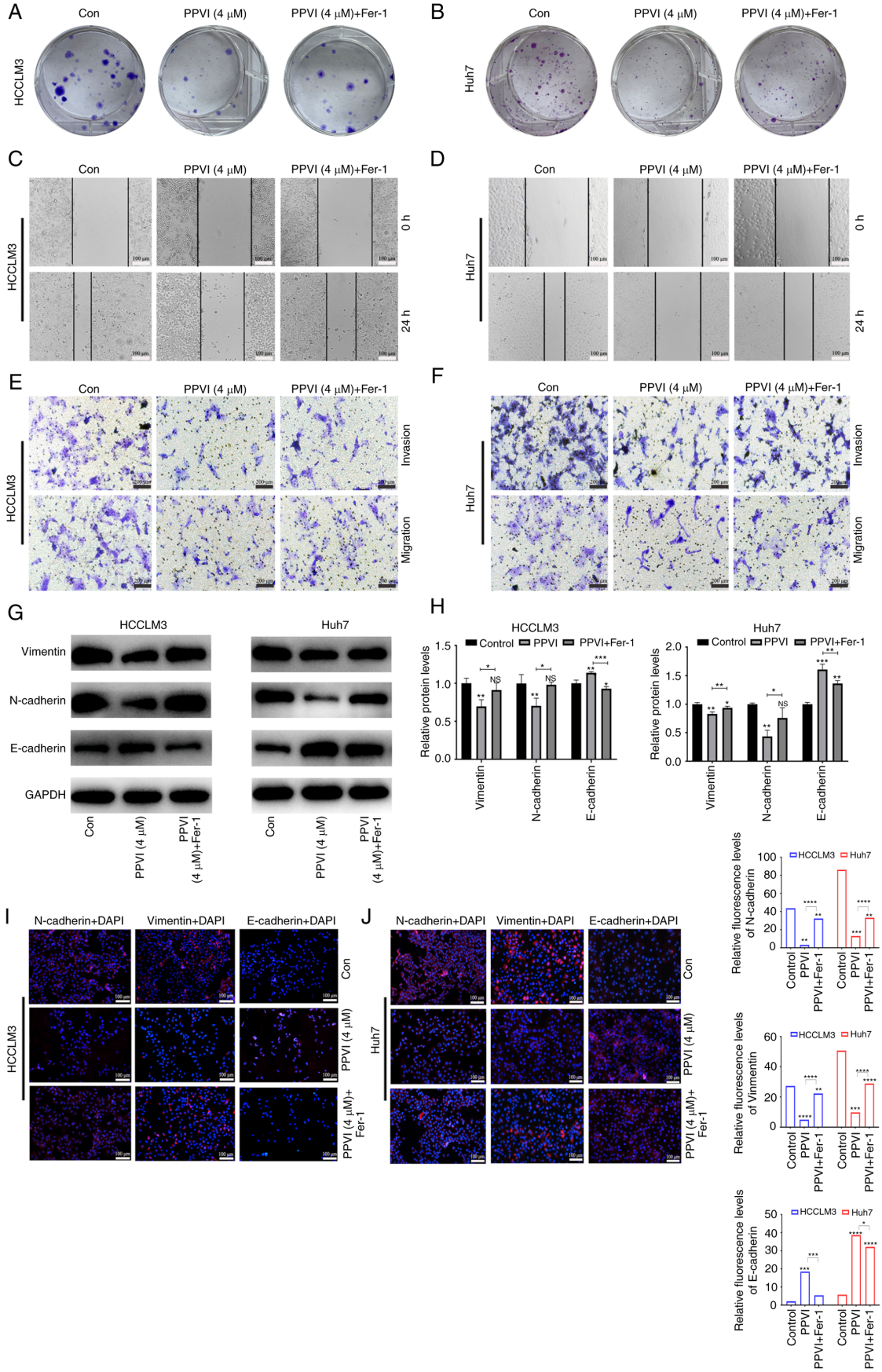

Figure 5. PPVI inhibits the invasion and migration of hepatocellular carcinoma cells by inducing ferroptosis. The HCCLM3 and Huh7 cells were treated with or without Fer-1 inhibitor for 2 h prior to treatment with PPVI for 24 h, after which different assays were performed. (A and B) Colony formation of cells treated with PPVI or PPVI + Fer-1. (C and D) Wound healing assay. (E and F) Transwell assay. (G and H) Western blot analysis of N-cadherin, Vimentin and E-cadherin protein expression in hepatocellular carcinoma cells. (I and J) The expression of N-cadherin, Vimentin and E-cadherin was detected using immunofluorescence staining. *P<0.05, **P<0.01, ***P<0.001 and ****P<0.0001 vs. control or as indicated. NS, not significant (vs. control); Con, control; PPVI, polyphyllin VI; Fer-1, ferrostatin-1.

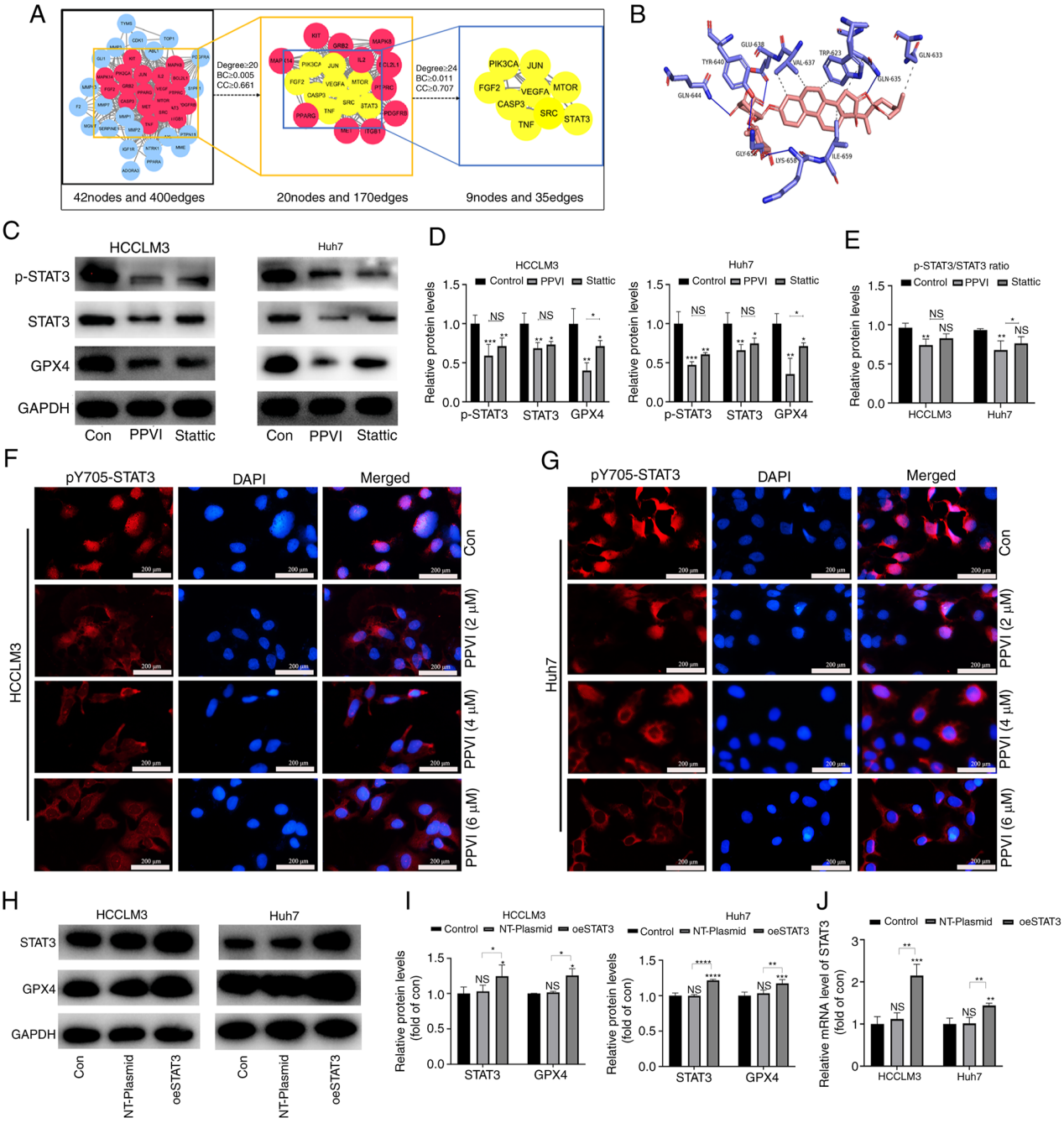

Figure 6. PPVI inhibits STAT3/GPX4 in hepatocellular carcinoma cells. (A) The binding activity between PPVI and STAT3 was examined using network pharmacology-based analysis and molecular docking technology. (B) Simulation of the combination of PPVI and STAT3. (C-E) HCCLM3 and Huh7 cells were treated with PPVI or Stattic for 24 h. Western blot analysis of GPX4, STAT3 and p-STAT3 protein expression in HCCLM3 and Huh7 cells. (F and G) Detection of pY705-STAT3 expression in HCCLM3 and Huh7 cells treated with PPVI (2, 4 and 6 μM) using immunofluorescence staining. (H and I) Western blot analysis of GPX4, STAT3 and p-STAT3 levels in HCC cells with or without the overexpression of STAT3. (J) RT-qPCR analysis of STAT3 mRNA expression. *P<0.05, **P<0.01, ***P<0.001 and ****P<0.0001 vs. control or as indicated. NS, not significant (vs. control); Con, control; PPVI, polyphyllin VI; STAT3, signal transducer and activator of transcription 3; GPX4, glutathione peroxidase 4; Fer-1, ferrostatin-1; oeSTAT3, STAT3 overexpression plasmid.

Morevoer, the phosphorylation ratio of STAT3 is presented in Fig. 7G. Similarly, the PPVI-induced decrease in the GPX4 mRNA levels was also reversed by STAT3 overexpression (Fig. 7H). Thus, PPVI induces ferroptosis by inhibiting the STAT3/GPX4 axis in HCC cells.

PPVI suppresses tumor growth in vivo via the STAT3/GPX4 axis. Subsequently, the present study investigated the mechanisms through which PPVI induces ferroptosis via regulation of the STAT3/GPX4 signaling pathway *in vivo*. Huh7 cells were injected subcutaneously into nude mice. Once the mice developed palpable tumors, the mice were treated for 10 consecutive days with intraperitoneal injections of PPVI, PPVI + Fer-1, or the same volume of saline (Fig. 8A and B). Fig. 8C shows that the weight of the mice in the saline group gradually decreased due to tumor consumption, while the body weight of the nude mice in the PPVI group decreased less than that in the PPVI + Fer-1 group. In the later period, the weight of the mice in the

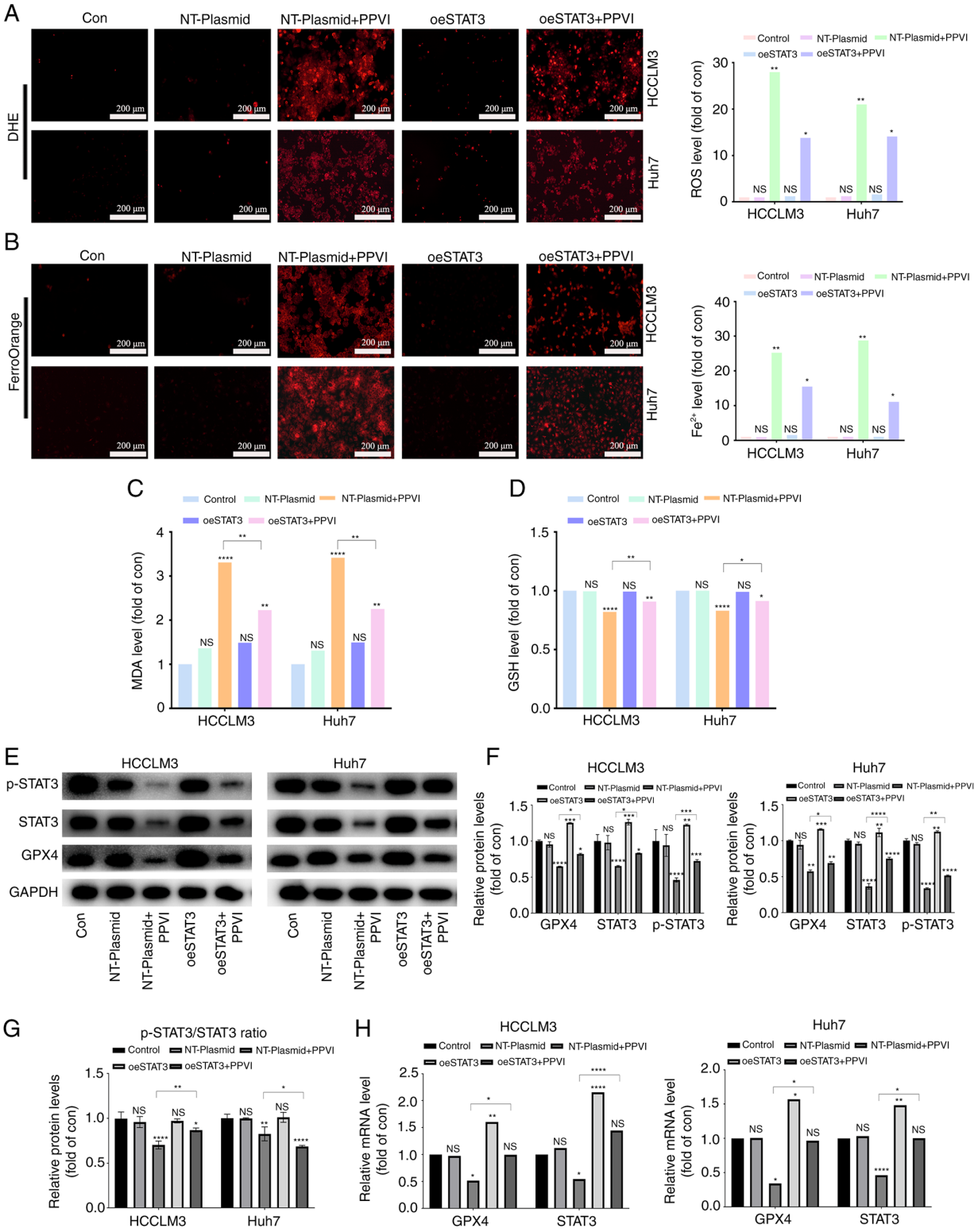

Figure 7. PPVI induces ferroptosis by inhibiting the STAT3/GPX4 axis in hepatocellular carcinoma cells. HCC cells with or without overexpression of STAT3 were treated with PPVI. (A) ROS levels in HCCLM3 and Huh7 cells were observed using DHE. (B) Fe^{2+} content in HCCLM3 and Huh7 cells was detected using the FerroOrange fluorescent probe. (C and D) MDA and GSH levels. (E-G) Protein expression of GPX4, p-STAT3 and STAT3 in HCCLM3 and Huh7 cells was detected using western blot analysis. (H) RT-qPCR analysis of STAT3 and GPX4 mRNA expression. *P<0.05, **P<0.01, ***P<0.001 and ****P<0.0001 vs. control or as indicated. NS, not significant (vs. control); Con, control; PPVI, polyphyllin VI; STAT3, signal transducer and activator of transcription 3; GPX4, glutathione peroxidase 4; oeSTAT3, STAT3 overexpression plasmid; DHE, dihydroethidium.

saline group exceeded that of the PPVI + Fer-1 group, which was deemed to be due to an increase in tumor net weight. PPVI suppressed tumor growth and the ferroptosis inhibitor, Fer-1, reversed this effect (Fig. 8D and E). Subsequently, liver function was examined by measuring the ALT and AST levels in mouse serum; the levels of PPVI and PPVI + Fer-1

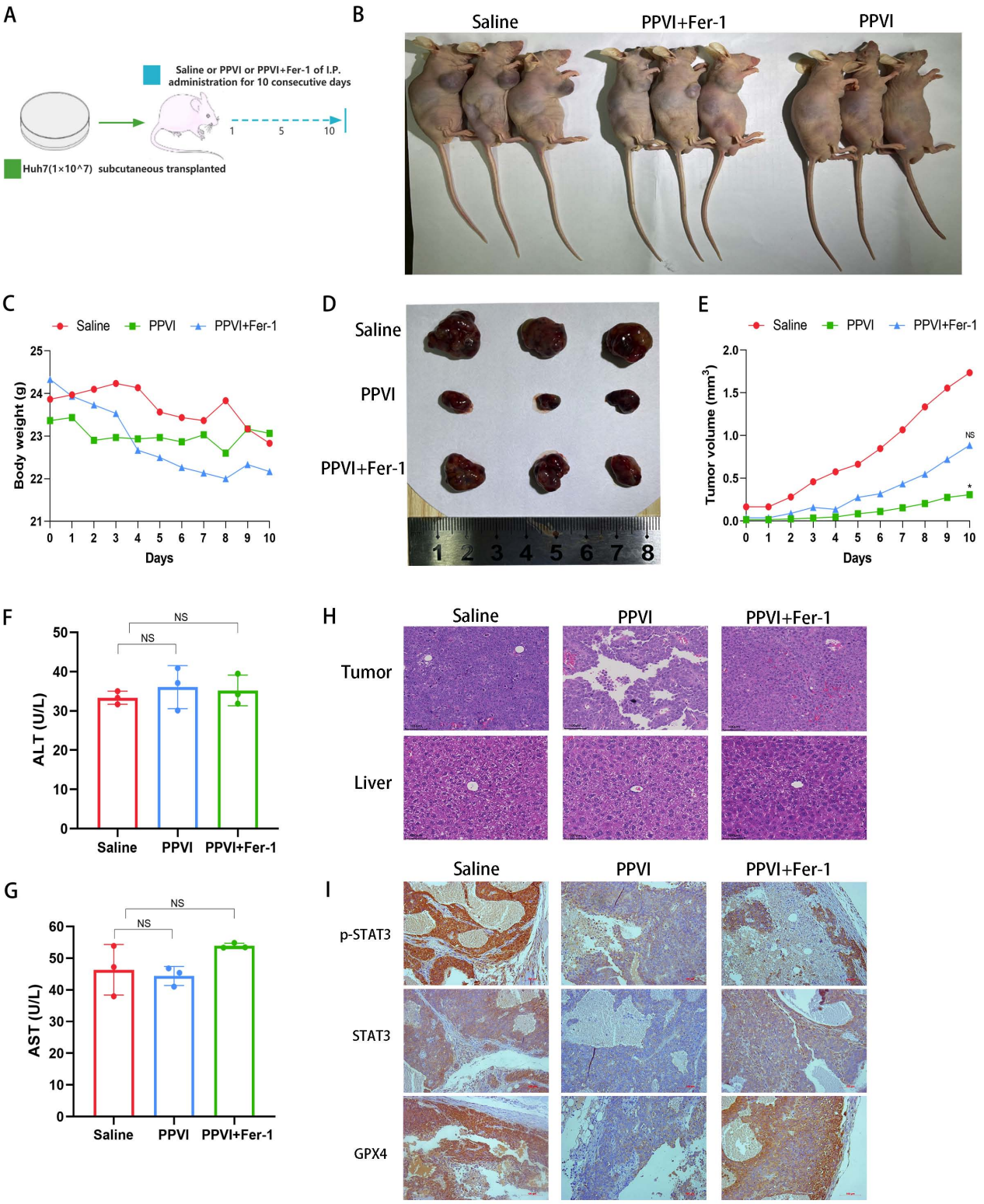

Figure 8. PPVI suppresses tumor growth *in vivo* through the STAT3/GPX4 axis. (A) Schematic diagram of the *in vivo* experiment. (B) Image of mice with subcutaneous tumor xenografts. (C) Muse weight. (D) Images of subcutaneous xenograft mouse tumors. (E) Changes in tumor volume in mice during drug injection. (F and G) The levels of ALT and AST, which are markers of liver function, were measured. (H) Hematoxylin and eosin staining illustrating the morphology of mouse liver and tumor tissue. (I) The level of p-STAT3, STAT3 and GPX4 proteins in the indicated tumor tissue was using immunohistochemistry. *P<0.05 vs. saline group. NS, not significant; PPVI, polyphyllin VI; STAT3, signal transducer and activator of transcription 3; GPX4, glutathione peroxidase 4; Fer-1, ferrostatin-1; AST, aspartate aminotransferase; ALT, alanine transaminase.

were not significantly altered compared to the control group (Fig. 8F and G). Furthermore, H&E staining of liver and tumor tissues revealed that PPVI exerted no evident hepatic damage and was thus a safe therapeutic agent (Fig. 8H). The results of immunohistochemistry revealed that Fer-1 reversed the decrease in the expression of p-STAT3, STAT3 and GPX4 in

the tumor mouse tissues (Fig. 8I). These data demonstrate the efficacy of PPVI in the treatment of liver cancer *in vivo* and indicate that PPVI exerts its effects via the STAT3/GPX4 axis.

Discussion

HCC presents a global health challenge with its increasing morbidity and mortality (2). Exhaustive research on HCC has led to considerable improvements being made the available monitoring methods and treatment strategies for this disease (3). However, the 5-year survival rate of patients remains poor (20%); chemotherapy remains the mainstay of treatment for patients with advanced-stage HCC, and sorafenib is the standard of care for these patients (3); however, it only provides patients with a limited survival benefit (3). Therefore, the development of more promising and therapeutically valuable HCC drugs, and the identification of innovative therapeutic targets, remain priorities. Current cancer therapies exert their anticancer effects by triggering cancer cell death, and small-molecule compounds targeting cancer cell death pathways are important and promising cancer treatment agents (16,17). The present study screened a library of small-molecule compounds of TCM monomers and identified a popular drug (PPVI), which was effective in inhibiting the proliferation, migration and invasion of HCC cells, potentially targeting the STAT3/GPX4 axis to induce ferroptosis.

The anticancer properties of PPVI have been demonstrated in various cancer models; for example, PPVI has been shown to induce the apoptosis of human osteosarcoma cells (14) and to induce NSCLC cell autophagic death via the ROS-mediated mTOR signaling pathway (18). However, the form of death induced by PPVI in HCC cells has not yet been reported, at least to the best of our knowledge. In the present study, PPVI treatment inhibited the viability of HCC cells. PPVI significantly reduced the number of viable HCC cells and their colony formation capacity. Furthermore, TEM revealed the typical morphological features of ferroptosis in HCC cells treated with PPVI, including a reduced mitochondrial volume and decreased or absent mitochondrial cristae. To further determine whether this form of cell death involved ferroptosis, the HCCLM3 and Huh7 cells were treated with PPVI in the absence or presence of several inhibitors of cell death. Fer-1 combination treatment prevented PPVI-induced cell death, suggesting that ferroptosis may be a key determinant of cell death in HCCLM3 and Huh7 cells treated with PPVI.

Ferroptosis is a new form of cell death discovered by Dixon *et al* (4) in 2012. It differs from necrosis, apoptosis and autophagy in genetics, biochemical characteristics and morphology (4). Chen *et al* (5) found that ferroptosis played a key role in tumor cytotoxicity and tumor progression. Several small molecules induce ferroptosis and exert tumor-suppressive effects in various experimental cancer models (19,20), involving mechanisms primarily related to iron overload, lipid peroxidation imbalance and cysteine transport (21). The accumulation of excess Fe^{2+} exerts potent oxidative effects through the Fenton reaction, which generates ROS and induces lipid peroxidation by reacting with polyunsaturated fatty acids on the lipid membrane (21). The present study found that the GSH levels in HCCLM3 and Huh7 cells gradually decreased, whereas the MDA, ROS and Fe^{2+} levels were significantly increased in a concentration-dependent manner following treatment with PPVI. Notably, Fer-1 not only alleviated the cellular mitochondrial damage induced by PPVI, but also reduced the biochemical characteristics of ferroptosis in HCC cells, including ROS accumulation and lipid peroxidation. These findings strongly suggest that ferroptosis contributes to the inhibitory effects of PPVI on the growth of HCC cells. The key to ferroptosis is lipid peroxidation, and GPX4 has been confirmed to play a crucial role in inhibiting iron-catalyzed lipid peroxidation in microsomes; this can be eliminated by reducing lipid hydroperoxides (22). For example, bufotalin has been shown to induce ferroptosis in NSCLC cells by accelerating the degradation of GPX4 and boosting intracellular Fe^{2+} (23). Furthermore, the phyto-sesquiterpene lactones, DET and DETD-35, have been found to induce ferroptosis in mutant melanoma through the inhibition of GPX4 (24). The findings of the present study are consistent with those of other research (25), demonstrating that GPX4 expression in HCC cells is negatively associated with the PPVI concentration. These findings provide new evidence of the anticancer effects of PPVI on HCC, particularly by the induction of ferroptosis.

EMT, the process by which epithelial cancer cells acquire a mesenchymal phenotype with metastatic and invasive properties, is one of the most critical events in cancer progression (26). It has been confirmed that drug-resistant cancer cells that normally undergo EMT are more likely to be killed by ferroptosis inducers. For example, β-elemene or cetuximab enhances the cytotoxic effects of RSL3 in KRAS-mutant colorectal cancer cells by improving RSL3-induced ferroptosis (27,28). To investigate whether PPVI can inhibit EMT in HCC cells by inducing ferroptosis, the present study detected several EMT-related markers using immunofluorescence staining and western blot analysis. The results revealed that PPVI increased the expression of the epithelial marker, E-cadherin, enhanced cell-cell adhesion junctions, and decreased the protein expression levels of N-cadherin and Vimentin in HCCLM3 and Huh7 cells, whereas the ferroptosis inhibitor, Fer-1, reversed these effects. These results suggest that PPVI inhibits EMT in HCC cells by inducing ferroptosis.

To clarify the mechanisms through which PPVI induces ferroptosis, nine core target proteins were identified by intersection screening based on the compound target database and the liver cancer target database. Using AutoDock molecular docking software, PPVI was found to target and regulate STAT3, an oxidation-responsive transcription factor that plays an active role in ferroptosis (29). In a previous study, treatment with a STAT3 inhibitor was found to enhance sensitivity to cisplatin by reactivating ferroptosis in cells (30). In another study, the inhibition of STAT3 downregulated SLC7A11, GPX4 and FTH1 expression to trigger ferroptosis, and inhibit tumor growth and reduce chemical resistance in gastric cancer (31). In addition, it was also previously demonstrated that impairing STAT3/Nrf2/GPx4 signaling induced ferroptosis and enhanced the sensitivity of osteosarcoma cells to cisplatin (32). In the present study, it was found that PPVI, similar to the STAT3 inhibitor, Stattic, inhibited the activation of STAT3, induced ferroptosis and reduced the levels of GPX4 in HCC cells, exerting

a significant antitumor effect. This is consistent with the conclusion of other researchers, in that Stattic can exert antitumor effects by inhibiting STAT3 phosphorylation and pancreatic cancer cell proliferation (33). In the present study, STAT3 was then overexpressed and it was confirmed that PPVI blocked GPX4 expression by inhibiting the phosphorylation of STAT3 through the accumulation of GSH, MDA and FE^{2+}, consistent with the findings of previous others (34). Finally, *in vivo* experiments revealed PPVI exerted anticancer effects with relative biosafety.

In conclusion, the present study demonstrates that the natural product, PPVI, is a novel ferroptosis inducer with the potential to induce ferroptosis and inhibit HCC cell metastasis and invasion. The present study discovered a novel mechanism of the anticancer effects of PPVI in HCC, which inhibits tumor growth by inhibiting the STAT3/GPX4 axis, inducing ferroptosis, and inhibiting the metastasis and invasion of HCC cells by regulating EMT. These data suggest PPVI may serve as a potential new drug for the treatment of HCC, and these data may thus provide a new direction for the treatment of HCC. However, the present study had certain limitations. First, it was not determined whether other molecular targets were involved and whether PPVI can bind to multi-target proteins involved in anticancer effects or ferroptosis. Second, other important molecular mechanisms through which STAT3 regulates the ferroptosis of HCC cells have not yet been identified. Thus, further studies are warranted to explore the multi-target proteins bound by PPVI, as well as the molecular mechanisms by which STAT3 regulates ferroptosis in HCC.

Acknowledgements

Not applicable.

Funding

The present study was supported by grants from the Shenzhen Science and Technology Project (Nos.JCYJ20210324120405015andJCYJ20180302173542393).

Availability of data and materials

The datasets used and/or analyzed during the current study are available from the corresponding author on reasonable request. The raw data and original images from the present study are included in the Figshare database (https://figshare.com/s/de9b1ad82b37321478c2). Further inquiries can be directed to the corresponding authors.

Authors' contributions

XZhou and ZH conceived the study and revised the manuscript. QH, JL and MM performed the experiments and drafted the original manuscript. ML, RH and XZhong participated in conducting the study and in data analysis. XS, JS and WF edited the manuscript and were involved in data curation. WM, WZ and BZ were responsible for the statistical analysis. QH and JL confirm the authenticity of all the raw data. All authors have read and approved the final version of the manuscript.

Ethics approval and consent to participate

All animal experiments were approved (No. 20220070) by the Animal Ethics Committee (AEC) of the China Science and Technology Industry Holdings (Shenzhen) Co., Ltd.

Patient consent for publication

Not applicable.

Competing interests

The authors declare that they have no competing interests.

References

1. Chidambaranathan-Reghupaty S, Fisher PB and Sarkar D: Hepatocellular carcinoma (HCC): Epidemiology, etiology and molecular classification. Adv Cancer Res 149: 1-61, 2021.
2. Sung H, Ferlay J, Siegel RL, Laversanne M, Soerjomataram I, Jemal A and Bray F: Global cancer statistics 2020: GLOBOCAN estimates of incidence and mortality worldwide for 36 cancers in 185 countries. CA Cancer J Clin 71: 209-249, 2021.
3. Cheng AL, Hsu C, Chan SL, Choo SP and Kudo M: Challenges of combination therapy with immune checkpoint inhibitors for hepatocellular carcinoma. J Hepatol 72: 307-319, 2020.
4. Dixon SJ, Lemberg KM, Lamprecht MR, Skouta R, Zaitsev EM, Gleason CE, Patel DN, Bauer AJ, Cantley AM, Yang WS, *et al*: Ferroptosis: An iron-dependent form of nonapoptotic cell death. Cell 149: 1060-1072, 2012.
5. Chen X, Kang R, Kroemer G and Tang D: Broadening horizons: The role of ferroptosis in cancer. Nat Rev Clin Oncol 18: 280-296, 2021.
6. Shan Y, Yang G, Huang H, Zhou Y, Hu X, Lu Q, Guo P, Hou J, Cao L, Tian F and Pan Q: Ubiquitin-like modifier activating Enzyme 1 as a novel diagnostic and prognostic indicator that correlates with ferroptosis and the malignant phenotypes of liver cancer cells. Front Oncol 10: 592413, 2020.
7. Wang K, Zhang Z, Tsai HI, Liu Y, Gao J, Wang M, Song L, Cao X, Xu Z, Chen H, *et al*: Branched-chain amino acid aminotransferase 2 regulates ferroptotic cell death in cancer cells. Cell Death Differ 28: 1222-1236, 2021.
8. Ye Z, Hu Q, Zhuo Q, Zhu Y, Fan G, Liu M, Sun Q, Zhang Z, Liu W, Xu W, *et al*: Abrogation of ARF6 promotes RSL3-induced ferroptosis and mitigates gemcitabine resistance in pancreatic cancer cells. Am J Cancer Res 10: 1182-1193, 2020.
9. Zhang H, Deng T, Liu R, Ning T, Yang H, Liu D, Zhang Q, Lin D, Ge S, Bai M, *et al*: CAF secreted miR-522 suppresses ferroptosis and promotes acquired chemo-resistance in gastric cancer. Mol Cancer 19: 43, 2020.
10. Xiang Y, Guo Z, Zhu P, Chen J and Huang Y: Traditional Chinese medicine as a cancer treatment: Modern perspectives of ancient but advanced science. Cancer Med 8: 1958-1975, 2019.
11. Liu C, Yang S, Wang K, Bao X, Liu Y, Zhou S, Liu H, Qiu Y, Wang T and Yu H: Alkaloids from traditional Chinese medicine against hepatocellular carcinoma. Biomed Pharmacother 120: 109543, 2019.
12. Teng JF, Mei QB, Zhou XG, Tang Y, Xiong R, Qiu WQ, Pan R, Law BY, Wong VK, Yu CL, *et al*: PPVI induces caspase-1-mediated pyroptosis via the induction of ROS/NF-κB/NLRP3/GSDMD signal axis in non-small cell lung cancer. Cancers (Basel) 12: 193, 2020.
13. Wang P, Yang Q, Du X, Chen Y and Zhang T: Targeted regulation of Rell2 by microRNA-18a is implicated in the anti-metastatic effect of polyphyllin VI in breast cancer cells. Eur J Pharmacol 851:161-173, 2019.
14. Yuan YL, Jiang N, Li ZY, Song ZZ, Yang ZH, Xue WH, Zhang XJ and Du Y: Polyphyllin VI induces apoptosis and autophagy in human osteosarcoma cells by modulation of ROS/JNK activation. Drug Des Devel Ther 13: 3091-3103, 2019.
15. Livak KJ and Schmittgen TD: Analysis of relative gene expression data using real-time quantitative PCR and the 2(-Delta Delta C(T)) method. Methods 25: 402-408, 2001.

16. Ke B, Tian M, Li J, Liu B and He G: Targeting programmed cell death using small-molecule compounds to improve potential cancer therapy. Med Res Rev 36: 983-1035, 2016.
17. Strasser A and Vaux DL: Cell death in the origin and treatment of cancer. Mol Cell 78: 1045-1054, 2020.
18. Teng JF, Qin DL, Mei QB, Qiu WQ, Pan R, Xiong R, Zhao Y, Law BY, Wong VK, Tang Y, *et al*: Polyphyllin VI, a saponin from Trillium tschonoskii Maxim. induces apoptotic and autophagic cell death via the ROS triggered mTOR signaling pathway in non-small cell lung cancer. Pharmacol Res 147: 104396, 2019.
19. Hassannia B, Vandenabeele P and Vanden Berghe T: Targeting ferroptosis to iron out cancer. Cancer Cell 35: 830-849, 2019.
20. Wu J, Ye J, Xie Q, Liu B and Liu M: Targeting regulated cell death with pharmacological small molecules: An update on autophagy-dependent cell death, ferroptosis, and necroptosis in cancer. J Med Chem 65: 2989-3001, 2022.
21. Su Y, Zhao B, Zhou L, Zhang Z, Shen Y, Lv H, AlQudsy LHH and Shang P: Ferroptosis, a novel pharmacological mechanism of anti-cancer drugs. Cancer Lett 483: 127-136, 2020.
22. Seibt TM, Proneth B and Conrad M: Role of GPX4 in ferroptosis and its pharmacological implication. Free Radic Biol Med 133: 144-152, 2019.
23. Zhang W, Jiang B, Liu Y, Xu L and Wan M: Bufotalin induces ferroptosis in non-small cell lung cancer cells by facilitating the ubiquitination and degradation of GPX4. Free Radic Biol Med 180: 75-84, 2022.
24. Chang MT, Tsai LC, Nakagawa-Goto K, Lee KH and Shyur LF: Phyto-sesquiterpene lactones DET and DETD-35 induce ferroptosis in vemurafenib sensitive and resistant melanoma via GPX4 inhibition and metabolic reprogramming. Pharmacol Res 178: 106148, 2022.
25. Zhang W, Gong M, Zhang W, Mo J, Zhang S, Zhu Z, Wang X, Zhang B, Qian W, Wu Z, *et al*: Thiostrepton induces ferroptosis in pancreatic cancer cells through STAT3/GPX4 signalling. Cell Death Dis 13: 630, 2022.
26. Bakir B, Chiarella AM, Pitarresi JR and Rustgi AK: EMT, MET, plasticity, and tumor metastasis. Trends Cell Biol 30: 764-776, 2020.
27. Chen P, Li X, Zhang R, Liu S, Xiang Y, Zhang M, Chen X, Pan T, Yan L, Feng J, *et al*: Combinative treatment of β-elemene and cetuximab is sensitive to KRAS mutant colorectal cancer cells by inducing ferroptosis and inhibiting epithelial-mesenchymal transformation. Theranostics 10: 5107-5119, 2020.
28. Yang J, Mo J, Dai J, Ye C, Cen W, Zheng X, Jiang L and Ye L: Cetuximab promotes RSL3-induced ferroptosis by suppressing the Nrf2/HO-1 signalling pathway in KRAS mutant colorectal cancer. Cell Death Dis 12: 1079, 2021.
29. Zhao Y, Wang C, Yang T, Wang H, Zhao S, Sun N, Chen Y, Zhang H and Fan H: Chlorogenic acid alleviates chronic stress-induced duodenal ferroptosis via the inhibition of the IL-6/JAK2/STAT3 signaling pathway in rats. J Agric Food Chem 70: 4353-4361, 2022.
30. Liu Q and Wang K: The induction of ferroptosis by impairing STAT3/Nrf2/GPx4 signaling enhances the sensitivity of osteosarcoma cells to cisplatin. Cell Biol Int 43: 1245-1256, 2019.
31. Ouyang S, Li H, Lou L, Huang Q, Zhang Z, Mo J, Li M, Lu J, Zhu K, Chu Y, *et al*: Inhibition of STAT3-ferroptosis negative regulatory axis suppresses tumor growth and alleviates chemoresistance in gastric cancer. Redox Biol 52: 102317, 2022.
32. Luo Y, Gao X, Zou L, Lei M, Feng J and Hu Z: Bavachin induces ferroptosis through the STAT3/P53/SLC7A11 axis in osteosarcoma cells. Oxid Med Cell Longev 2021: 1783485, 2021.
33. Guo H, Xiao Y, Yuan Z, Yang X, Chen J, Chen C, Wang M, Xie L, Chen Q, Tong Y, *et al*: Inhibition of $STAT3^{Y705}$ phosphorylation by Stattic suppresses proliferation and induces mitochondrial-dependent apoptosis in pancreatic cancer cells. Cell Death Discov 8: 116, 2022.
34. Gaschler MM, Andia AA, Liu H, Csuka JM, Hurlocker B, Vaiana CA, Heindel DW, Zuckerman DS, Bos PH, Reznik E, *et al*: $FINO_2$ initiates ferroptosis through GPX4 inactivation and iron oxidation. Nat Chem Biol 14: 507-515, 2018.